Article

Journal of Vibration and Control
2022, Vol. 28(17-18) 2310–2318

DOI: 10.1177/10775463211009988
journals.sagepub.com/home/jvc
SAGE

Proportional control moment gyroscope for two-wheeled self-balancing robot

Faruk Ünker

Abstract

A two-wheeled self-balancing robot is considered for investigating the responses of a control moment gyroscope powered by a proportional controller to prevent the robot rollover against the constant inertia forces because of accelerations of the wheels of the robot. The amplitudes of the frequency equations related to the required angular momentum of flywheels with an optimum controller gain were also found. A simulation model of the robot using computer-aided engineering software (RecurDyn) is built to verify the equations of a Lagrangian model. The results of both obtained from the Lagrangian and that from RecurDyn simulations are analyzed comparatively, in which the proportional control loop reduces the required flywheel speeds Ω of gyros and keeps the robot in a very small amplitude of a stable sinusoidal motion in the upright position.

Keywords

Inverted pendulum, gyroscope, gyrostabilizer, control moment gyroscope, proportional controller, two-wheeled self-balancing robot

1. Introduction

Over the last decade, robots gained in popularity from both academics and industrials because of their competitiveness, sustainability, and dangerous tasks (Korayem et al., 2012; Li and Li, 2021; Li et al., 2020). With the rapid development of robots in many industrial roles, people are seeking collaborative innovation between the mechanical structure and control algorithm for increasing reliability and precision (Korayem and Gariblu, 2003). In recent years, mobile robots have dramatically reduced energy consumption and increased the flexibility and velocity of motion under very complex and variable conditions (Korayem and Gariblu, 2004; Korayem et al., 2010). Wheeled mobile robots, unlike the legged robots, are relatively easy to control the kinematics with sophisticated equipment and have a simple design (Imtiaz et al., 2018; Larimi et al., 2015; Takei et al., 2009).

A two-wheeled self-balancing robot has a growing interest based on one common engineering problem of an inverted pendulum (Irdayanti et al., 2020). Thanks to their high maneuverability, small size, and simple and compact structures (Imtiaz et al., 2018; Takei et al., 2009), two-wheeled self-balancing robots perform well in transportation applications (Grasser et al., 2002). A well-known two-wheel robot Segway has been the most famous commercial vehicle for personal transportation purposes (http://segway.com).

There are several methods for a mobile inverted pendulum robot to balance at the upright position such as moving the wheel(s) of the pendulum horizontally (Hosoda et al., 2006; Irdayanti et al., 2020) and using a reaction wheel (Larimi et al., 2015) and a control moment gyro (CMG) (Park and Cho, 2018; Tanaka and Nagasawa, 2020; Yun et al., 2020). The disadvantage of moving the wheel(s) and tilting its body to provide stability of the center of gravity is that the magnitude of the disturbance can cause the robot to fall (Xu et al., 2016). Besides, a conventional inverted pendulum robot does not perfectly provide safety even though consisting of complex electromechanical systems with robust control algorithms developed for stability (Lin et al., 2011; Ruan and Chen, 2010). To overcome this limitation, an inertia wheel can be used by accelerating or decelerating a flywheel to generate a torque on the lateral axis. Because inertia wheels cannot balance with a constant angular velocity, they are less stable and have less torque

Department of Mechanical Engineering, Gümüşhane University, Turkey

Received: 21 January 2021; accepted: 24 March 2021

Corresponding author:
Faruk Ünker, Department of Mechanical Engineering, Gümüşhane University, Bağlarbaşı, Gumushane 29100, Turkey.
Email: farukunker@gumushane.edu.tr

ability compared with the control moment gyroscope (CMG).

CMG has been widely used to stabilize the unbalanced structure via tilting the gimbal of a rotating flywheel (Defendini et al., 2003; Ünker, 2020; Wasiwitono et al., 2020; Yetkin and Ozguner, 2013). The precession effects of the CMG were used for two-wheeled self-balancing robots to produce more precise and stronger torque than the reaction wheel to prevent the robot from falling (Park and Cho, 2018) and to have better maneuverability (Chen et al., 2016). This controllable torque can be a constant and applied against constant inertia forces because of the accelerations of the robot (Mahvan and Akbarzadeh, 2015). However, the CMG cannot provide stability for a long period of time because of a constant flywheel's rotational velocity. Because the larger angle of the gimbal results in less torque and needs a high rotational velocity of flywheels for a stable balancing against continuous (constant) disturbances, the roll angle of the gimbal should be kept as small as possible.

In this article, a novel method is introduced for balancing a two-wheeled self-balancing robot against continuous (constant) disturbances by using a CMG based on the proportional (P) control loop. This new method proposes that the CMG can provide stability for a long period of time with a fewer and constant rotational velocity of the flywheel despite a larger angle of the gimbal. There is another torque regulated by a proportional (P) controller as the control output to stabilize the roll angle of the gimbal, in which each gimbal has the reverse inputs to eliminate the reaction torques on the body of the robot. As the gimbal of the rotating flywheel is tilted by the proportional (P) controller, certain modes of two sinusoidal motions occur. As a result, the sinusoidal gimbal motion induces a very small amplitude of sinusoidal motion of the robot in the upright position. Therefore, the proportional (P) control loop maintains the balance of the robot with a stable continuous period. Besides, the comparisons show that the theoretical results of the Lagrangian equations agree well with the RecurDyn ones.

2. System setup

The two-wheeled self-balancing robot is composed of two gimbals containing two gyroscopic flywheels moving in opposite directions to each other to keep the body in its vertical position and to eliminate the unwanted reaction torques. The precession of the rotating flywheel is controlled by tilting control torque produced by a P-controller using a measured gimbal angle. To control twin gimbals of gyros, the measurement of the roll angle of the gimbal is fed back to the controller again because gimbal's roll angle is the most important parameter of the torque which produces the counter torque required to balance the pitch motion of the robot in the upright position within a small pitch angle of a sinusoidal motion.

Symmetrical on the left and right sides, there are two spinning flywheels connected with their own rotatable gimbals to the robot body as shown in Figure 1. As shown in Figure 2, the whole assembly of flywheels and the gimbals is rotating in opposite directions about their own pivot axis which is positioned in a plane midway in the body of the robot. The angular displacements of the gimbals become -θ and θ, respectively, and the gimbals can be assumed to have one degree of freedom when the flywheels are spinning with the same angular velocities. Therefore, this article is based on the equations of motion, written in the form of three differential equations (7–9) of three degrees of freedom with the unknowns z, θ, and φ, respectively. The descriptions and physical properties of the system are given in Table 1.

3. Equations of motion of two-wheeled self-balancing robot

A simplified model of a two-wheeled self-balancing robot with two gyros is shown in Figure 2. The kinetic energies of the flywheel, gimbal, wheel, and the robot body can be defined as follows, respectively

$$T_{\text{flywheel}} = \frac{1}{2} m_d z^2 + \frac{1}{2} I_o \left(\dot{\theta}^2 + \dot{\varphi}^2 \cos^2\theta\right) + \frac{1}{2} I_p (\Omega + \dot{\varphi} \sin\theta)^2 \tag{1}$$

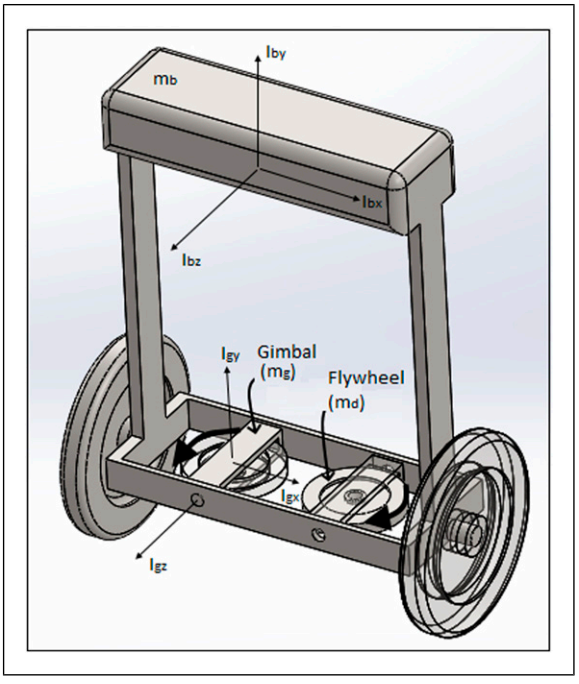

Figure 1. Physical model of the two-wheeled robot.

$$T_{\text{gimbal}} = \frac{1}{2}m_g\dot{z}^2 + \frac{1}{2}I_{gx}\dot{\varphi}^2\cos^2\theta + \frac{1}{2}I_{gy}\dot{\varphi}^2\sin^2\theta + \frac{1}{2}I_{gz}\dot{\theta}^2 \tag{2}$$

$$T_{\text{wheel}} = \frac{1}{2}m_w\dot{z}^2 + \frac{1}{2}I_w\left(\frac{\dot{z}}{r}\right)^2 \tag{3}$$

$$T_{\text{body}} = \frac{1}{2}m_b\left[(-L\dot{\varphi}\sin\varphi)^2 + (L\dot{\varphi}\cos\varphi + \dot{z})^2\right] + \frac{1}{2}I_{bx}\dot{\varphi}^2 \tag{4}$$

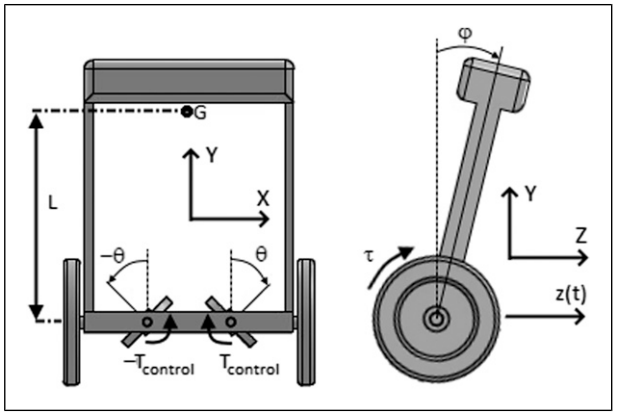

Figure 2. Two-wheeled robot via a balance arm of body mass, m_b, with length of the centroid (G).

Therefore, the total kinetic energy of the robot can be obtained as

$$T_{\text{total}} = 2T_{\text{flywheel}} + 2T_{\text{gimbal}} + 2T_{\text{wheel}} + T_{\text{body}} \tag{5}$$

The center of mass of gyros is located at the pivot point of the robot's body (inverted pendulum) as zero potential energy. Therefore, the total potential energy of the robot is

$$V_{\text{total}} = m_b g L\cos\varphi \tag{6}$$

Therefore, Lagrange's equations become

$$\frac{d}{dt}\left(\frac{\partial T_{\text{total}}}{\partial \dot{z}}\right) - \frac{\partial T_{\text{total}}}{\partial z} + \frac{\partial V_{\text{total}}}{\partial z} = \frac{2\tau}{r} \tag{7}$$

$$\frac{d}{dt}\left(\frac{\partial T_{\text{total}}}{\partial \dot{\theta}}\right) - \frac{\partial T_{\text{total}}}{\partial \theta} + \frac{\partial V_{\text{total}}}{\partial \theta} = 2T_{\text{control}} \tag{8}$$

$$\frac{d}{dt}\left(\frac{\partial T_{\text{total}}}{\partial \dot{\varphi}}\right) - \frac{\partial T_{\text{total}}}{\partial \varphi} + \frac{\partial V_{\text{total}}}{\partial \varphi} = -2\tau \tag{9}$$

By applying Lagrange's equations, the nonlinear equations of motion can be obtained as follows

$$\left(M_t + \frac{2I_w}{r^2}\right)\ddot{z} + m_b L\ddot{\varphi}\cos\varphi - m_b L\dot{\varphi}^2\sin\varphi = \frac{2\tau}{r} \tag{10}$$

Table 1. Physical properties of the two-wheeled robot.

Symbol	Numerical values	Description
g	9.80665 m/s^2	Gravitational acceleration
r	0.15 m	Radius of the wheel
L	0.48513349 m	Length of the centroid of the body mass
m_b	77.6601705 kg	Body mass
m_g	1.66864601 kg	Mass of each gimbal
m_w	15.1349604 kg	Mass of each wheel
m_d	2.16404683 kg	Flywheel mass of each gyroscope
I_p	0.00703616 kg m^2	The rotary inertia of each flywheel
I_o	0.00357619 kg m^2	Mass moment of inertia of each flywheel
I_{gx}	0.00573533 kg m^2	Principal moments of inertia of each gimbal
I_{gy}	0.00572707 kg m^2	Principal moments of inertia of each gimbal
I_{gz}	0.00066736 kg m^2	Principal moments of inertia of each gimbal
I_{bx}	3.01987954 kg m^2	Principal moments of inertia of body
I_w	0.20812696 kg m^2	The rotary inertia of the wheel
Ω	1000–2500 rad/s	Rotating speed of each flywheel
τ	0.5 N m	The torque for each wheel
P	1–1.5	The proportional gain for each gimbal

$$\left(I_o + I_{gz}\right)\ddot{\theta} + \left(I_o - I_p + I_{gx} - I_{gy}\right)\dot{\varphi}^2 \cos\theta \sin\theta - I_p\Omega\dot{\varphi}\cos\theta = P\theta; \tag{11}$$

$$\left(2I_o\cos^2\theta + 2I_p\sin^2\theta + 2I_{gx}\cos^2\theta + 2I_{gy}\sin^2\theta + I_{bx} + m_bL^2\right)\ddot{\varphi} + 4\left(I_p - I_o + I_{gy} - I_{gx}\right)\dot{\varphi}\dot{\theta}\sin\theta\cos\theta + 2I_p\Omega\dot{\theta}\cos\theta + \ddot{z}m_bL\cos\varphi - m_bgL\sin\varphi = -2\tau \tag{12}$$

where

$$M_t = 2m_d + 2m_g + 2m_w + m_b \tag{13}$$

3.1. Reduced equations of motion about the equilibrium position for small vibration of body

Suppose that a harmonic gimbal motion is required to balance the robot with an acceleration because of the wheels' moment. So the pitch angle of the robot φ(t) should be investigated as a harmonic function. Then, the responses may be chosen as an angular frequency ω

$$\theta(t) = -\theta_0\sin(\omega t) \tag{14}$$

$$\varphi(t) = \varphi_0[1 - \cos(\omega t)] \tag{15}$$

As seen from equation (15), pitch velocity is always zero ($\dot{\varphi} = 0$) for the zero pitch displacement ($\varphi = 0$). Then, the pitch acceleration should have a very small value ($\ddot{\varphi} \approx 0$) with a low frequency according to equations (10) and (15). One will obtain that a body acceleration ($\ddot{z} = a$) occurs for a small amplitude ($\varphi_0 \approx 0$ and $\cos\varphi_0 = 1$ and $\sin\varphi_0 = \varphi_0$) of the pitch vibrations. Then, equation (10) can be reduced into the following form

$$\ddot{z} = a = \frac{2\tau}{r(M_t + (2I_w/r^2))} \tag{16}$$

For the zero pitch acceleration ($\ddot{\varphi} = 0$), neglecting the terms of a higher power for $\dot{\varphi} \approx 0$ near to the body's equilibrium position at the gimbal's zero roll ($\theta \approx 0$ and $\cos\theta = 1$), equations (11) and (12) can be reduced to

$$\left(I_o + I_{gz}\right)\omega^2\theta_0 - I_p\Omega\omega\varphi_0 = -P\theta_0 \tag{17}$$

$$-2I_p\Omega\omega\theta_0\cos(\omega t) + am_bL - m_bgL\varphi_0[1 - \cos(\omega t)] = -2\tau \tag{18}$$

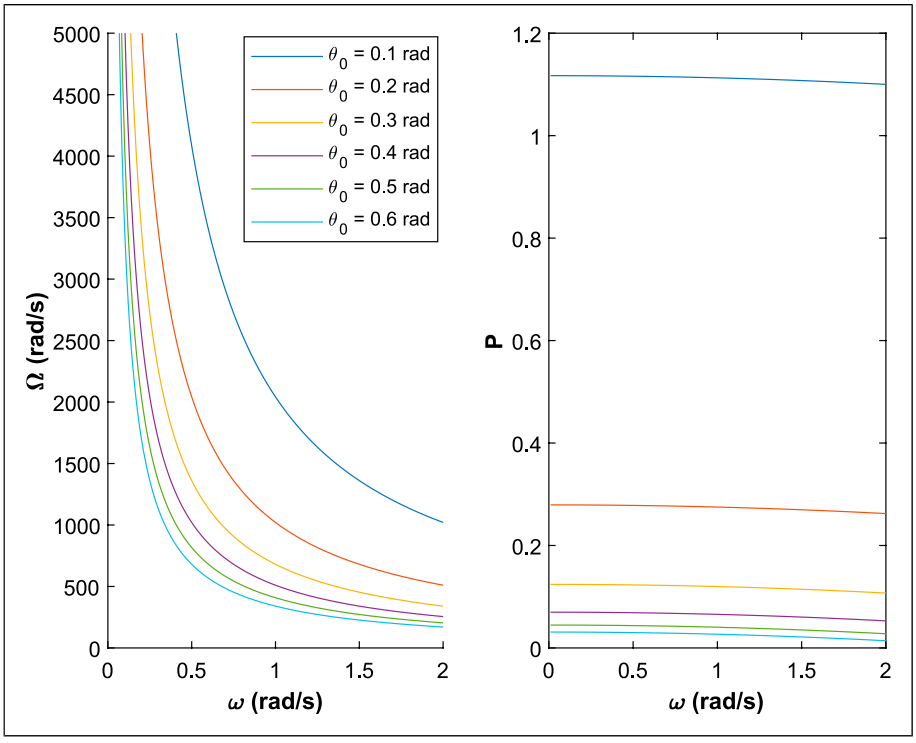

Figure 3. Effect of the frequency, ω, on the flywheel speed, Ω, and the proportional gain, P.

Hence, by solving these equations, one can obtain the roll amplitude of gimbal, the pitch amplitude of body, and the frequency as follows

$$\theta_0 = \frac{m_b L}{2 I_p \Omega \omega}\left(a + \frac{2\tau}{m_b L}\right); \tag{19}$$

$$\varphi_0 = \frac{1}{g}\left(a + \frac{2\tau}{m_b L}\right) \tag{20}$$

$$\omega = \sqrt{\frac{m_b g L P}{2\left(I_p \Omega\right)^2 - m_b g L\left(I_o + I_{gz}\right)}} \tag{21}$$

Equation (20) shows that pitch amplitude relates to the torque of wheels. Besides, equations (19) and (21) can be rearranged as

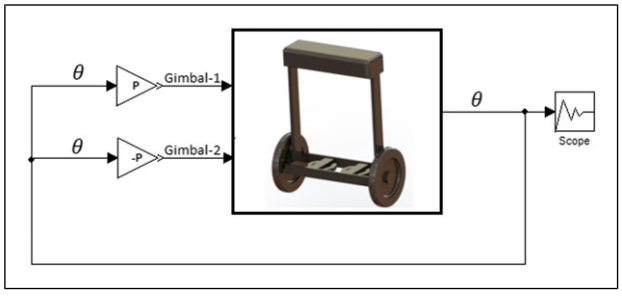

Figure 4. Controller schematic diagram.

$$\Omega = \frac{m_b L}{2 I_p \omega \theta_0}\left(a + \frac{2\tau}{m_b L}\right) \tag{22}$$

$$P = \frac{\omega^2\left[2\left(I_p \Omega\right)^2 - m_b g L\left(I_o + I_{gz}\right)\right]}{m_b g L} \tag{23}$$

Hence, the optimum P gain coefficient of the controller can be determined through these equations although the original equations of motion are nonlinear. Using Equations (22) and (23), the P-gains for a small frequency ω with as possible as low flywheel speed Ω can be obtained for a required amplitude of roll angle θ_0 as seen in Figure 3.

4. Results

In the two-wheeled self-balancing robot, the roll angle of a gimbal is taken as the input of the P-controller, whereas the output of the controller is the moment to balance the gimbal as seen in Figure 4. An optimum proportional gain of the P-controller for a minimum flywheel speed can be determined through equations (22) and (23). In the following calculations, equations (10)–(12) with the physical parameters given in Table 1 can be solved by using MATLAB software using the fourth-order Runge–Kutta method. To identify the dynamical behavior of the model given in Figures 1, 2, and 4, time responses were simulated with the time step size of 0.001 s and zero initial conditions.

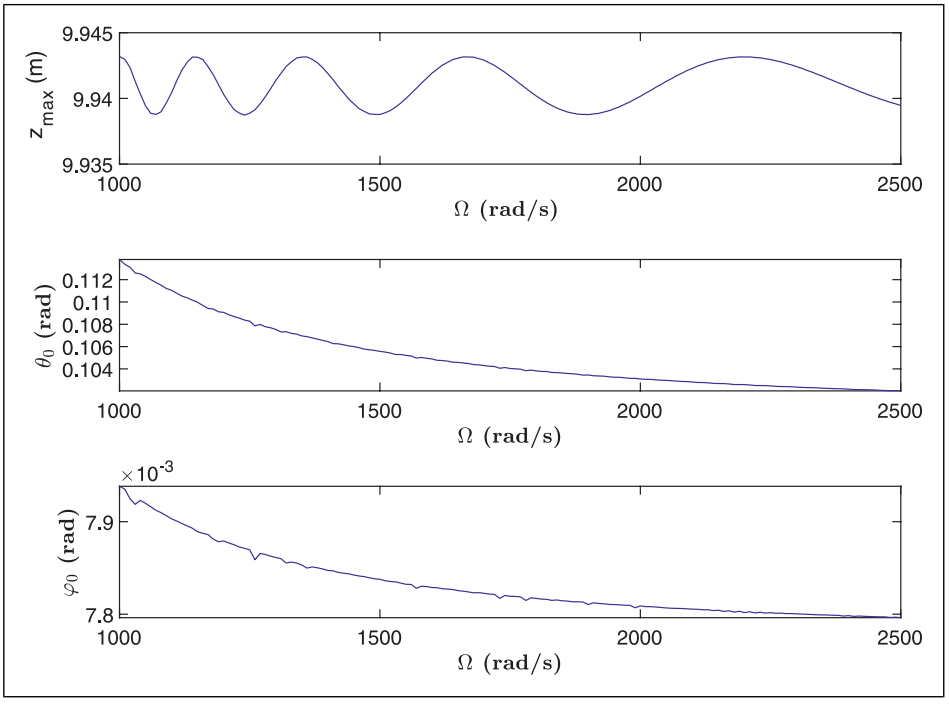

Figure 5. Effect of the flywheel speed Ω for P = 1.113.

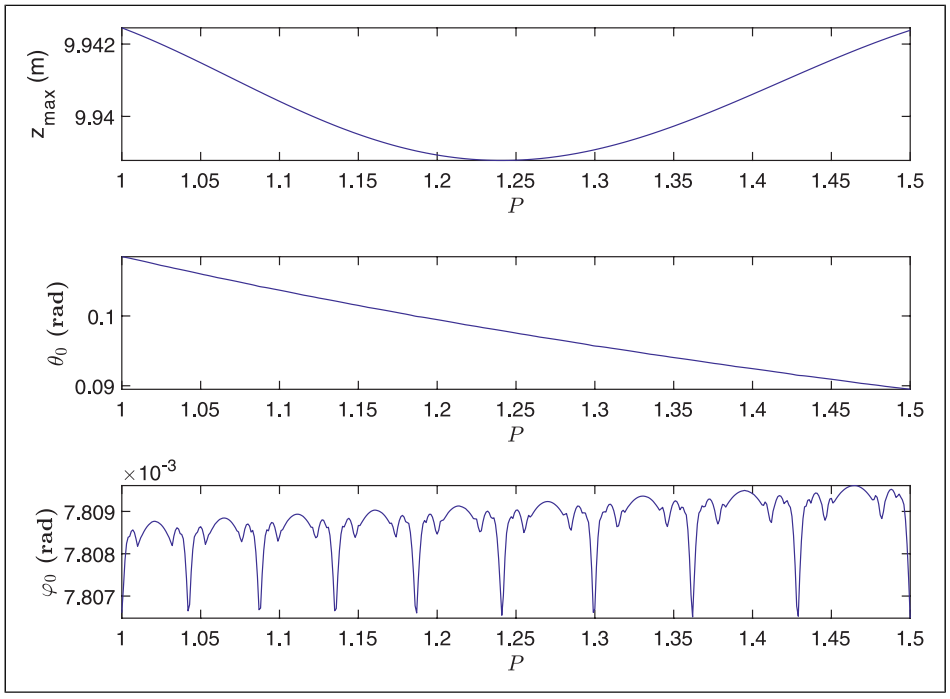

Figure 6. Effect of the proportional gain P for Ω = 2000 rad/s.

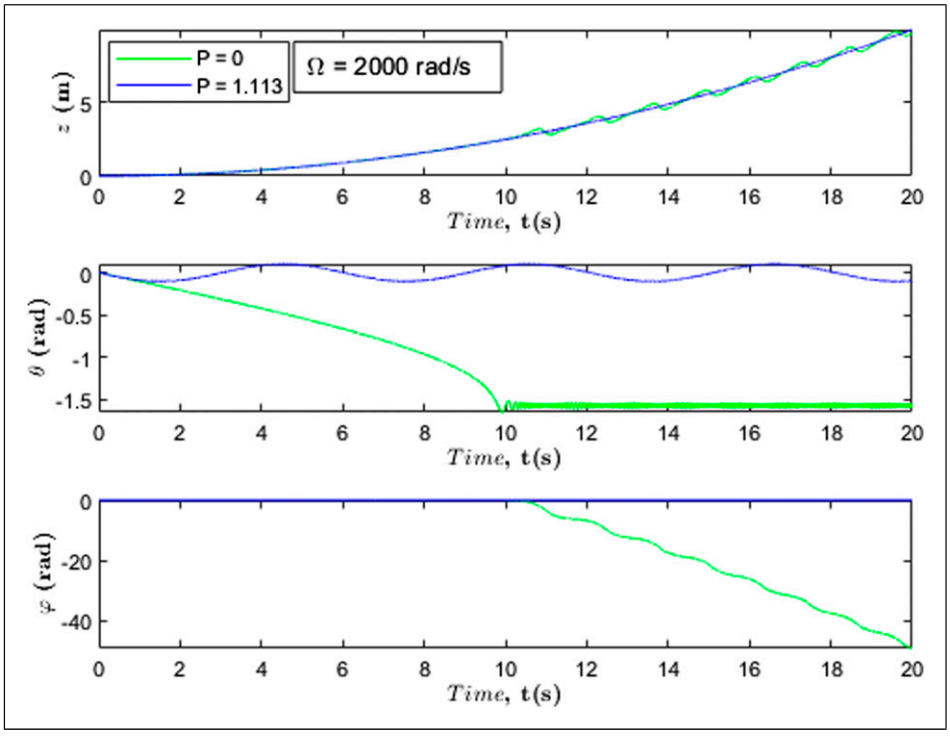

Figure 7. Time response curves for different proportional gains (P) with the frequency ω = 1.02 rad/s and the flywheel speed Ω = 2000 rad/s.

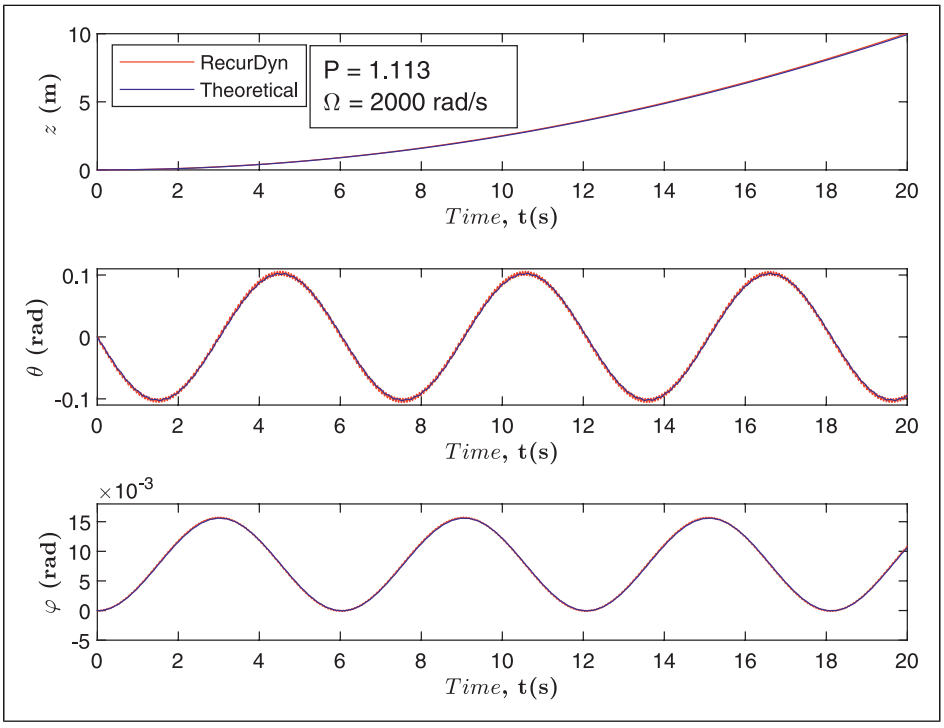

Figure 8. Comparison of RecurDyn computer-aided engineering software and the theoretical results for the frequency ω = 1.02 rad/s with θ_0 = 0.1 rad.

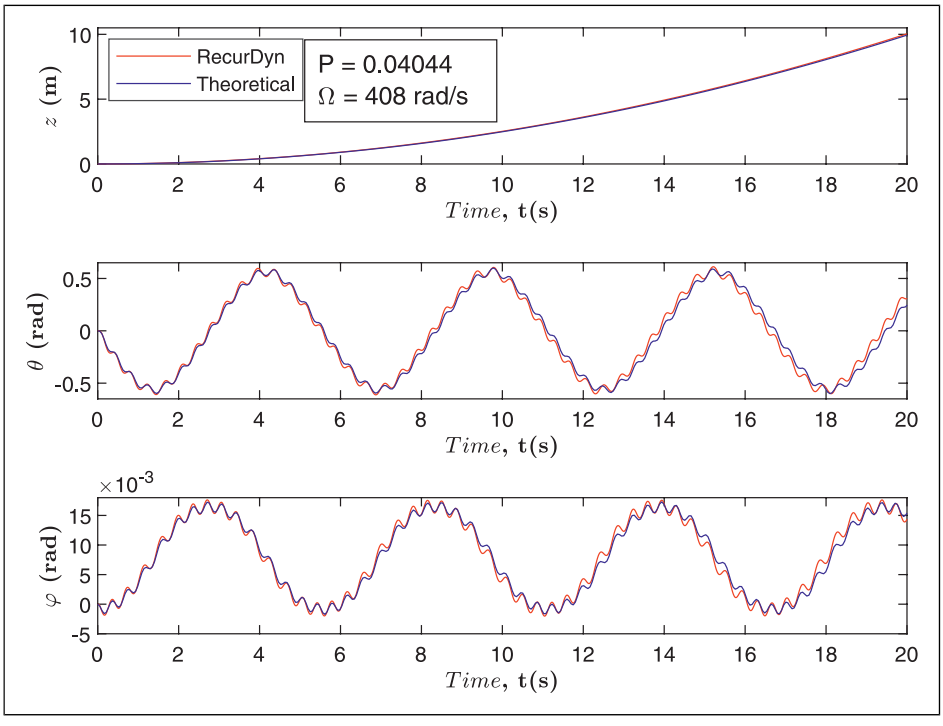

Figure 9. Comparison of RecurDyn computer-aided engineering software and the theoretical results for the frequency ω = 1.02 rad/s with θ_0 = 0.5 rad.

Furthermore, the correctness of the theoretical results may be verified by CAE software (RecurDyn).

Figure 5 illustrates Lagrange's results for the varying flywheel speeds of the gyro for P = 1.113 selected from Figure 3. In Figure 5, the flywheel angular velocity was kept constant with the linear rate of 10 rad/s during each sweeping. The maximum displacement of 20 s was determined during each sweep. When rotor speed has higher values, which means more control moment of the gyro, the roll amplitude of gimbal θ_0 decreases while the body (z_{max}, φ_0) runs into robust motion.

Figure 6 represents the P-response curves of the displacements at Ω = 2000 rad/s selected from Figure 3. For Figure 6, time responses for 20 s were simulated, and maximum responses were determined during each constant sweeping gain with a linear sweep rate of 0.001. The peaks of pitch amplitude φ_0 decrease while increasing the roll amplitude of gimbal θ_0 at the low level of P. The pitch mitigation performance can be improved using an optimum P-control gain at the high level of roll angle θ of gimbals.

The uncontrolled (P = 0) and controlled (P = 1.113) time responses of the displacements from the calculated results of Lagrange's equations are shown in Figure 7. The results for the frequency ω = 1.02 rad/s and the flywheel speed Ω = 2000 rad/s show that with controlling the CMG, the gain P = 1.113 keeps the body at a steady-state oscillation of φ. However, the uncontrolled CMG (P = 0) loses control after 10 s because it reached the equilibrium position at $\theta = \pi/2$. With a constant flywheel velocity, the uncontrolled CMG cannot balance the robot's body under the continuous disturbance torque because of equation (24) derived from equations (10) and (12). So, the φ-displacement response of the robot can be controlled when an optimum P-controller is used

$$\Omega = \frac{1}{2I_p \sin\theta} \int \left\{ -2\tau \left[1 + \frac{m_b L}{r(M_t + (2I_w/r^2))} \right] + m_b g L \varphi \right\} dt \tag{24}$$

In Figures 8 and 9, the simulated results of Lagrange's equations were compared with the results obtained from the RecurDyn. The comparisons of robot's and gimbal's displacements are analyzed that the theoretical and RecurDyn results are stable and almost the same for the frequency ω = 1.02 rad/s. Besides, it can be deduced from the comparisons that the tendencies of the results agreed well with Figure 3 obtained from equations (22) and (23) for θ_0=0.1 and 0.5 rad, respectively. Meanwhile, similar results can be also obtained from equations (14)–(16). When the roll amplitude of gimbal θ_0 has higher values, the flywheel needs less angular velocity. However, the roll amplitude of gimbal θ_0 should be selected as small as possible for a stable motion.

5. Conclusion

In this article, a CMG-controlled two-wheeled self-balancing robot is designed for traveling fast on a flat road under the continuous disturbance acceleration because of wheels' torque. The P-controller has been implemented to solve the problem of conventional gyros in maintaining constant moments with a constant angular velocity of the flywheel. The P-controller stabilizes the gimbal's motion to increase the performance of keeping the main body in its vertical position. The dynamic mathematical model of the robot with the gyrostabilizers is derived using the Lagrangian formulation, and the correlations have been determined from equations of motions. The simulation results indicate that the robot can accelerate without losing its balance using the P-controlled CMG. The performance significantly depends on the flywheel speed and the precession tilted by the P-controller. Furthermore, the correctness of the theoretical results is verified by CAE software and shows that the CAE results agree well with the theoretical results.

Declaration of Conflicting Interests

The author(s) declared no potential conflicts of interest with respect to the research, authorship, and/or publication of this article.

Funding

The author(s) received no financial support for the research, authorship, and/or publication of this article.

ORCID iD

Faruk Ünker https://orcid.org/0000-0002-9709-321X

References

Chen J, Ye P, Sun H, et al. (2016) Design and motion control of a spherical robot with control moment gyroscope. In: IEEE international conference on systems and informatics, 19–21 November 2016. Shangai, China: IEEE.

Defendini A, Faucheux P, Guay P, et al. (2003) Control moment GYRO CMG 15-45 S: a compact CMG product for agile satellites in the one ton class. In: 10th European space mechanisms and tribology symposium, 24–36 September 2003, pp. 27–31. San Sebastián, Spain: ESA.

Grasser F, D'Arrigo A, Colombi S, et al. (2002) JOE: a mobile, inverted pendulum. *IEEE Transactions on Industrial Electronics* 49(1): 107–114.

Hosoda Y, Egawa S, Tamamoto J, et al. (2006) Basic design of human-symbiotic robot EMIEW. In: International conference on intelligent robots and systems, 9–15 October 2006, 5079–5084. Beijing, China: IEEE.

Imtiaz MA, Naveed M, Bibi N, et al. (2018) Control system design, analysis & implementation of two wheeled self balancing robot. In: 9th Annual information technology, electronics and mobile communication conference – IEMCON 2018, 1–3 November 2018, 1–6. Vancouver, Canada: IEEE.

Irdayanti Y, Kusumanto RD, Anisah M, et al. (2020) Ultrasonic sensor application as a performance enhancement of robot two wheels. *Journal of Physics: Conference Series* 1500: 012007.

Korayem MH and Ghariblu H (2003) Maximum allowable load on wheeled mobile manipulators imposing redundancy constraints. *Robotics and Autonomous Systems* 44: 151–159.

Korayem MH and Gariblu H (2004) Analysis of wheeled mobile flexible manipulator dynamic motions with maximum load carrying capacities. *Robotics and Autonomous Systems* 48(2–3): 63–76.

Korayem MH, Azimirad V, Nikoobin A, et al. (2010) Maximum allowable load of autonomous mobile manipulator in environment with obstacle considering tip over stability. *International Journal of Advanced Manufacturing Technology* 46(5–8): 811–829.

Korayem MH, Azimirad V, Vatanjou H, et al. (2012) Maximum load determination of nonholonomic mobile manipulator using hierarchical optimal control. *Robotica* 30(1): 53–65.

Larimi SR, Zarafshan P and Moosavian SAA (2015) A new stabilization algorithm for a two-wheeled mobile robot aided by reaction wheel. *Journal of Dynamic Systems, Measurement, and Control* 137(1): 011009.

Li Z and Li S (2021) Saturated PI control for nonlinear system with provable convergence: an optimization perspective. *IEEE Transactions on Circuits and Systems II: Express Briefs* 68(2): 742–746.

Li Z, Li C, Li S, et al. (2020) A fault-tolerant method for motion planning of industrial redundant manipulator. *IEEE Transactions on Industrial Informatics* 16(12): 7469–7478.

Lin S-C, Tsai C-C and Huang H-C (2011) Adaptive robust self-balancing and steering of a two-wheeled human transportation vehicle. *Journal of Intelligent & Robotic Systems* 62(1): 103–123.

Mahvan A and Akbarzadeh A (2015) Gyro stabilized two-wheeled inverted pendulum robot. In: Proceedings of the 3rd RSI international conference on robotics and mechatronics, 7–9 October 2015, 669–674. Tehran, Iran: IEEE.

Park J-H and Cho B-K (2018) Development of a self-balancing robot with a control moment gyroscope. *International Journal of Advanced Robotic Systems* 15: 1–11.

Ruan X and Chen J (2010) H1 robust control of self-balancing two wheeled robot. In: 8th World congress on intelligent control and automation, 7–9 July 2010, 6524–6527. Jinan, China: IEEE.

Takei T, Imamura R and Yuta S (2009) Baggage transportation and navigation by a wheeled inverted pendulum mobile robot. *IEEE Transactions on Industrial Electronics* 56(10): 3985–3994.

Tanaka K and Nagasawa S (2020) Posture stability control of a small inverted pendulum robot in trajectory tracking using a control moment gyro. *Advanced Robotics* 34(9): 610–620.

Ünker F (2020) Tuned gyro-pendulum stabilizer for control of vibrations in structures. *The International Journal of Acoustics and Vibration* 25(3): 355–362.

Wasiwitono U, Wahjudi A and Saputra AK (2020) Stabilization and disturbance attenuation control of the gyroscopic inverted pendulum. *Journal of Vibration and Control* 27(3–4): 415–425.

Xu J, Shang S, Qi H, et al. (2016) Simulative investigation on head injuries of electric self-balancing scooter riders subject to ground impact. *Accident Analysis & Prevention* 89: 128–141.

Yetkin H and Ozguner U (2013) Stabilizing control of an autonomous bicycle. In: 9th Asian control conference (ASCC), 23–26 June 2013, pp. 1–6. Istanbul, Turkey: IEEE.

Yun SY, Lee WS and Gwak K-W (2020) CMG-based anthropomorphic test device for human rider behavior reproduction for two-wheeled self-balancing personal mobility. *Mechatronics* 69: 102365.

Appendix

Notation

a	the acceleration of robot along Z direction
G	the center of mass of body
g	the gravitational acceleration
I_p	the rotary inertia of each flywheel
I_o	the mass moment of inertia of each flywheel
I_{gx}, I_{gy}, I_{gz}	the principal moments of inertia of each gimbal (taken at the center of mass of each gimbal)
I_{bx}, I_{by}, I_{bz}	the principal moments of inertia of body (taken at the center of mass of the body)
I_w	the rotary inertia of each wheel
L	the length of the centroid of the body mass
m_b	the body mass
m_g	the mass of each gimbal
m_w	the mass of each wheel
m_d	the flywheel mass of each gyroscope
M_t	total mass of two-wheeled robot
P	the proportional gain of controller
r	the radius of each wheel
$T_{control}$	the control output torque exerted to each gimbal
T_{body}	the kinetic energy of body
T_{gimbal}	the kinetic energy of each gimbal
$T_{flywheel}$	the kinetic energy of each flywheel
T_{wheel}	the kinetic energy of each wheel
T_{total}	total kinetic energy of two-wheeled robot
V_{total}	total potential energy of two-wheeled robot
(X, Y, Z)	the coordination in the world coordination system
z	the linear displacement of robot along Z direction
z_{max}	the maximum displacement of robot along Z direction
θ	the roll angle displacement of each gimbal
θ_0	the amplitude of roll angle displacement of each gimbal
φ	the head (pitch) angle displacement of body
φ_0	the amplitude of pitch angle displacement of body
ω	the angular frequency of each gimbal's harmonic motion
Ω	the rotational velocity of each flywheel
τ	the torque exerted to each wheel